HAL
archives-ouvertes.fr

Co-design of aircraft vertical tail and control laws using distributed electric propulsion

Eric Nguyen Van, Daniel Alazard, Philippe Pastor, Carsten Döll

▶ To cite this version:

Eric Nguyen Van, Daniel Alazard, Philippe Pastor, Carsten Döll. Co-design of aircraft vertical tail and control laws using distributed electric propulsion. IFAC Symposium on Automatic Control in Aerospace, Aug 2019, CRANFIELD, United Kingdom. hal-02355242

HAL Id: hal-02355242

https://hal.archives-ouvertes.fr/hal-02355242

Submitted on 8 Nov 2019

Co-design of aircraft vertical tail and control laws using distributed electric propulsion [⋆]

E. Nguyen Van [∗,∗∗] **D. Alazard** [∗] **P. Pastor** [∗] **C. Döll** [∗∗]

∗ *Institut Supérieur de l'Aéronautique et de l'Espace*
(eric.nguyen-van@isae.fr).
∗∗ *ONERA, The French Aerospace Lab (carsten.doll@onera.fr)*

Abstract: Distributed Electric Propulsion is investigated as a way to increase directional control of aircraft and reduce the vertical tail surface area. A co-design approach is presented where a H_∞ control method is used to both synthesize longitudinal/lateral control law gains and allocation module while sizing the vertical tail surface area and the propeller actuator bandwidth. The variation of the vertical tail surface area is captured throughout a collection of linearized aircraft systems representing different sizes of the vertical tail reassembled in a Linear Fractional Representation. This approach allows a reduction of 60% of the vertical tail surface area while maintaining desired dynamic behaviors with low actuator bandwidth.

Keywords: Distributed Electric Propulsion, Differential Thrust, Co-design, H_∞ control, vertical tail sizing, actuator bandwidth

1. INTRODUCTION

Distributed Electric Propulsion allows more flexible airframe propulsion integration and exploitation of favorable synergy between propulsion, aerodynamic or flight control as presented by Felder et al. (2009), Hermetz et al. (2016) and Schmollgruber et al. (2019). This study lies in the context of increase of control authority made possible by active differential thrust. In previous studies, it has been shown that the use of differential thrust necessitates a reduction in vertical tail surface area to increase the flight envelop, see Nguyen-Van et al. (2018b). Additionally, with a distributed propulsion, the consequences of one engine failure are less critical and allows to reduce the vertical tail surface area while remaining compliant with flight safety, see Nguyen-Van et al. (2018a). These studies showed the interest of differential thrust in the reduction of vertical tail. Remains the question of how much to reduce the vertical tail given a certain distributed propulsion.
A co-design approach similar to Denieul et al. (2017) is selected to minimize the vertical tail while designing the longitudinal/lateral control laws and the engine allocation module. The optimization procedure includes also a minimization of the engine bandwidth which is a determining parameter for differential propulsion control since the presumed low engine bandwidth, with respect to classical control surface bandwidths, could bring loss of control authority. In this approach, the vertical tail surface area is thought as a linearly varying parameter. Optimization tools available for robust control techniques are then used to handle the variation of matrices with the variation of vertical tail surface area and allows the minimization of control gains, engine bandwidth and vertical tail surface area under longitudinal/lateral handling quality constraints.

The second section describes the aircraft configuration considered in this study and the derivation of its linear model, parameterized according to the vertical tail surface. The model dynamics are analyzed for a given flight operating condition selected for its relevance regarding the design of distributed propulsion control. The third section describes the co-design problem and optimization process based on a multi-step optimization. The fourth section presents the obtained results. Conclusions and perspectives are summarized in the last section.

2. DETERMINATION OF LINEARIZED SYSTEMS

In this section, the procedure to obtain the Linear Fractional Representation of an aircraft with the vertical tail as varying parameter is explained.

2.1 Aircraft Equations of Motion

The equations of flight in the aerodynamic frame, assuming uniform wind velocity are used. Equations are derived in Boiffier (1998) and are presented here in a compact form for the sake of brevity. The interested reader is referred to Boiffier (1998) and Nguyen-Van et al. (2018b) for a more detailed treatment. Let $\boldsymbol{A}$ be the acceleration vector and $\boldsymbol{\Omega}$ the vector of rotation rates, the equations of motion write:

$$m\boldsymbol{A} = m\boldsymbol{g} + \boldsymbol{F}_A + \boldsymbol{F}_T, \qquad (1)$$

$$\mathbf{I}\dot{\boldsymbol{\Omega}} + \boldsymbol{\Omega} \times \mathbf{I}\boldsymbol{\Omega} = \boldsymbol{M}_A + \boldsymbol{M}_T, \qquad (2)$$

with m the mass, $\boldsymbol{g}$ the gravity vector, $\mathbf{I}$ the inertia matrix, $\boldsymbol{F}_A$, $\boldsymbol{F}_T$ and $\boldsymbol{M}_A$, $\boldsymbol{M}_T$ are respectively the force and torque vectors due to aerodynamic and engines thrust.

Developing the acceleration term, $\boldsymbol{A}$, while assuming zero wind velocity, allows to rewrite equation (1) as:

$$m\dot{\boldsymbol{V}} + \mathbf{T}_{ab}\boldsymbol{\Omega} \times \boldsymbol{V} = m\boldsymbol{g} + \boldsymbol{F}_A + \boldsymbol{F}_T, \qquad (3)$$

where $\mathbf{T}_{ab}$ is the rotation matrix between the body carried frame and the aerodynamic frame and $\boldsymbol{V}$ is the velocity vector in the aerodynamic frame. Equation (3) allows to explicit the state variables: V, α, β, being the airspeed, the angle of attack and the side slip angle, and p, q and r, the roll, pitch and yaw rates:

$$m\begin{pmatrix} \dot{V} \\ \dot{\beta}V \\ \dot{\alpha}V\cos\beta \end{pmatrix} + \mathbf{T}_{ab}\begin{pmatrix} p \\ q \\ r \end{pmatrix} \times \boldsymbol{V} = m\boldsymbol{g} + \boldsymbol{F}_A + \boldsymbol{F}_T, \qquad (4)$$

$$\mathbf{I}\begin{pmatrix} \dot{p} \\ \dot{q} \\ \dot{r} \end{pmatrix} + \begin{pmatrix} p \\ q \\ r \end{pmatrix} \times \mathbf{I}\begin{pmatrix} p \\ q \\ r \end{pmatrix} = \boldsymbol{M}_A + \boldsymbol{M}_T. \qquad (5)$$

The complementary kinematic equations for the Euler angles: bank ϕ, pitch θ and heading ψ are :

$$\begin{pmatrix} \dot{\phi} \\ \dot{\theta} \\ \dot{\psi} \end{pmatrix} = \begin{pmatrix} 1 & \sin\phi\tan\theta & \cos\phi\tan\theta \\ 0 & \cos\phi & -\sin\phi \\ 0 & \dfrac{\sin\phi}{\cos\theta} & \dfrac{\cos\phi}{\cos\theta} \end{pmatrix} \begin{pmatrix} p \\ q \\ r \end{pmatrix}. \qquad (6)$$

Two additional parameters are necessary to find pseudo-equilibriums: the flight path angle γ and the turn rate Ω. For steady turns Ω is equal to the rate of change of heading and using the last line of equation (6):

$$\begin{aligned} \sin\gamma &= \cos\alpha\cos\beta\sin\theta - \sin\beta\sin\phi\cos\theta \\ &\quad - \sin\alpha\cos\beta\cos\phi\cos\theta, \end{aligned} \qquad (7)$$

$$\Omega = (q\sin\phi + r\cos\phi)\frac{1}{\cos\theta}. \qquad (8)$$

Leaving aside the last row of system (6), the system to solve consists in equations (4), (5), (6), (7) and (8) representing a set of $N_e = 10$ equations. The state vector is $\mathbf{x} = [V, \alpha, \beta, p, q, r, \phi, \theta]^T$ and counts $n_x = 8$ variables. The directional control being entirely made with differential thrust, the input vector corresponding to control surfaces is composed of ailerons and elevator deflection: $\mathbf{u} = [\delta_a, \delta_e]^T$ with $n_u = 2$. Finally, $n_p = 2$ additional parameters γ and Ω are counted.
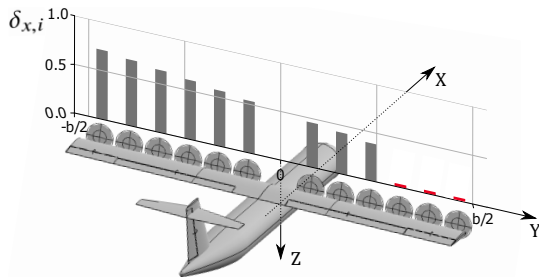

Fig. 1. Illustration of thrust distribution on the reference aircraft with twelve electric engines.

2.2 Reference Aircraft

Commuter and regional aircraft are often cited as the next big step in developing electric airplanes since most of their missions are within the limits of electric propulsion in terms of endurance, see Moore and Fredericks (2014) and Stückl (2015). A good representative of this class of aircraft is the ATR72 which details are reported in table 1.

Table 1. ATR 72 general details. See ATR (2015) and Jackson (2015)

Variables	Value
Wingspan (b)	27m
Wing surface area (S)	61m^2
Vertical tail surface area (S_{v_0})	12 m^2
Mass (m)	22800Kg
Total available power	4000KW
Stall velocity V_s	56m/s

For the configuration with distributed electric propulsion, the number of engines N is set to twelve. They are equally distributed along the leading edge as represented in Fig 1. The total available power for the electric engines, P_E, is identical to the original power: $P_E = 4000$KW. The only varying geometrical parameter is the vertical tail surface area S_v.

The aerodynamic derivatives required to model this aircraft are determined using a Vortex Lattice Method included in OpenVSP, see Gloudemans et al. (1996).

2.3 Propulsion modeling

Engine lines of thrust are assumed to be aligned with the aircraft X body axis and contained within the X-Y plan so that no pitching moment is induced by the thrust. Rotor terms or gyroscopic effects due to elements in rotations are assumed negligible such that equations of flight are not further modified. Thrust force and torque produced by differential thrust are calculated by summation of the contribution of each engine based on the geometrical arrangement shown in Fig 1:

$$\boldsymbol{F}_{T_b} = \begin{pmatrix} \displaystyle\sum_{i=1}^{N} F_{T,i}(\delta_{x,i}) \\ 0 \\ 0 \end{pmatrix}, \quad \boldsymbol{M}_T = \begin{pmatrix} 0 \\ 0 \\ \displaystyle\sum_{i=1}^{N} \text{-}F_{T,i}(\delta_{x,i})y_i \end{pmatrix}, \qquad (9)$$

where $F_T(\delta_{x,i})$ is the thrust produced by the ith engine located at a distance y_i from the body X-axis, with the throttle command: $\delta_{x,i}$. Engines are numbered starting from the outer left wing ($-b/2$) to the outer right wing ($b/2$). The term used in equation (4) is obtained by projecting equation (9) on the aerodynamic frame:

$$\boldsymbol{F}_T = \mathbf{T}_{ab}\boldsymbol{F}_{T_b}. \qquad (10)$$

For electric motors, the following thrust model may be considered for estimating $F_{T,i}(\delta_{x,i})$ following Sachs (2012):

$$F_{T,i}(\delta_{x,i}) = \frac{P_E}{N}V^{-1}\eta_m\eta_p\delta_{x,i}, \qquad (11)$$

with η_m and η_p respectively the engine and propeller efficiency (both considered constant). Therefore, the power is equally divided between the N engines. Finally, $\delta_{x,i}$ is added to the control input vector : $\mathbf{u} = [\delta_a, \delta_e, \delta_{x,1}, \ldots, \delta_{x,N}]^T$. The number of inputs becomes : $n_u = N + 2 = 14$.

2.4 Finding the trim position by optimization

A possible way to find an equilibrium is given by Goman et al. (2008). However, due to the high number of actuators

present in this case, the number of variables ($n_x + n_u = 22$) is higher than the number of equations ($N_e = 10$) and constraints. Therefore, an optimisation method is used to find a solution to this over-determined problem such as suggested by Oppenheimer and David B Doman (2006).

Flight conditions are set by adding constraints to fix the following variables: $[V, \beta, \gamma, \Omega]$. The objective function to minimise is defined as the power required to maintain equilibrium.

Finally, bounds are added on control inputs to remain within acceptable ranges of deflection or power levels.

The problem hence writes:

$$\min_{\tilde{x}} \ \sum_{i=1}^{N} F_{T,i}(\delta_{x,i}) V, \tag{12}$$

with: $\quad \tilde{x} = [\alpha, p, q, r, \phi, \theta, \delta_a, \delta_e, \delta_{x,1}, \ldots, \delta_{x,N}]^T$,
such that:

$$m\boldsymbol{g} + \boldsymbol{F}_A + \boldsymbol{F}_T - \mathbf{T}_{ab} \begin{pmatrix} p \\ q \\ r \end{pmatrix} \times \boldsymbol{V} = 0, \tag{13}$$

$$\boldsymbol{M}_A + \boldsymbol{M}_T - \begin{pmatrix} p \\ q \\ r \end{pmatrix} \times \mathbf{I} \begin{pmatrix} p \\ q \\ r \end{pmatrix} = 0, \tag{14}$$

$$0 = p + q \sin\phi \tan\theta + r \cos\phi \tan\theta, \tag{15}$$
$$0 = q \cos\phi - r \sin\phi, \tag{16}$$
$$\Omega = (q \sin\phi + r \cos\phi) / \cos\theta, \tag{17}$$
$$\sin\gamma = \cos\alpha \cos\beta \sin\theta - \sin\beta \sin\phi \cos\theta$$
$$\quad - \sin\alpha \cos\beta \cos\phi \cos\theta. \tag{18}$$

A Sequential Least SQuares Programming algorithm available in SciPy, see Kraft (1988), is used to solve the optimization problem with a tolerance set to 10^{-6} on the constraints.

2.5 Linearisation

The system is linearised by a first order TAYLOR expansion of the system. Equations 4, 5 and 6 form a system of non linear equations of the form:
$$\dot{\mathbf{x}} = \boldsymbol{f}(\mathbf{x}, \boldsymbol{u}), \tag{19}$$
with
$$\mathbf{x} = [V, \beta, \alpha, p, q, r, \phi, \theta]^T, \tag{20}$$
$$\mathbf{u} = [\delta_a, \delta_e, \delta_{x,1}, \ldots, \delta_{x,i}, \ldots, \delta_{x,12}]^T. \tag{21}$$
The solution $\hat{\mathbf{x}}$ of the optimisation problem (12) and the fixed parameters $[V, \beta, \gamma, \Omega]$ are used to reconstruct the state and input vectors: $\hat{\mathbf{x}}$, $\hat{\mathbf{u}}$ with values at equilibrium. The Jacobian of $\boldsymbol{f}(\mathbf{x}, \mathbf{u})$ is evaluated numerically by computing centered finite differences:

$$\dot{\tilde{\mathbf{x}}} = \frac{\partial \boldsymbol{f}}{\partial \mathbf{x}} \tilde{\mathbf{x}} + \frac{\partial \boldsymbol{f}}{\partial \mathbf{u}} \tilde{\mathbf{u}}, \tag{22}$$

with $\tilde{\mathbf{x}} = \mathbf{x} - \hat{\mathbf{x}}$ and $\tilde{\mathbf{u}} = \mathbf{u} - \hat{\mathbf{u}}$.

It is of interest to introduce the flight path angle γ in the state space representation so as to better differentiate the short period oscillation (mainly α and q dynamics) and the phugoid (mainly V and γ dynamics). One can do so by a variable change: using equation (7), small angle assumption and neglecting terms of second order, the pitch angle can be expressed as:

$$\theta = \gamma + \alpha, \quad \text{thus:} \ \dot{\theta} = \dot{\gamma} + \dot{\alpha}. \tag{23}$$

Substracting the line corresponding to $\dot{\alpha}$ in the matrices $\frac{\partial \boldsymbol{f}}{\partial \mathbf{x}}$, $\frac{\partial \boldsymbol{f}}{\partial \mathbf{u}}$ completes the reformulation. Finally, the system is re-ordered and can be decoupled to obtain:

$$\dot{\mathbf{x}}_L = \mathbf{A}_L \mathbf{x}_L + \mathbf{B}_L \mathbf{u}_L, \tag{24}$$
$$\dot{\mathbf{x}}_D = \mathbf{A}_D \mathbf{x}_D + \mathbf{B}_D \mathbf{u}_D, \tag{25}$$

with:

$$\mathbf{x}_L = [\widetilde{V}, \widetilde{\gamma}, \widetilde{\alpha}, \widetilde{q}]^T, \tag{26}$$
$$\mathbf{u}_L = [\widetilde{\delta}_e, \widetilde{\delta}_{x,1}, \ldots, \widetilde{\delta}_{x,12}]^T, \tag{27}$$
$$\mathbf{x}_D = [\widetilde{\beta}, \widetilde{p}, \widetilde{r}, \widetilde{\phi}]^T, \tag{28}$$
$$\mathbf{u}_D = [\widetilde{\delta}_a, \widetilde{\delta}_{x,1}, \ldots, \widetilde{\delta}_{x,12}]^T, \tag{29}$$

and the additional notation: $\widetilde{\boldsymbol{\delta}}_x = [\widetilde{\delta}_{x,1}, \ldots, \widetilde{\delta}_{x,12}]^T$.

2.6 Variation of the Vertical Tail Surface Area

Capturing the effect of geometrical changes in the vertical tail surface area is a tedious problem because of the important influence of other aircraft components on the flow impacting the vertical tail. This has been demonstrated by Fabrizio Nicolosi (2013) as a motivation for the construction of a semi-empirical model (VeDSC) accounting for fuselage and horizontal tail geometry to predict vertical tail performances. For a detailed presentation of VeDSC and its inclusion in the model, the reader is referred to Ciliberti et al. (2013) and Nguyen-Van et al. (2018b).

After inclusion in the aircraft aerodynamic model, the VeDSC method allows the computation of a collection of linearised systems, each system representing a different size of the vertical tail. It further permits the investigation of the reduction of the surface area on the aircraft lateral dynamics as presented in Fig 2. This result is obtained for the flight condition $[V, \beta, \gamma, \Omega] = [1.3V_s = 68\text{m/s}, 0°, 0°, 0°/s]$ which was selected as particularly sizing for differential thrust control. Indeed, at $1.3V_s$, the pilot requires a wide flight envelop while the control efficiency of propulsion is inversely proportional to the velocity, see equation (11) and Nguyen-Van et al. (2018a). As the vertical tail reduces, the side slip oscillation gradually becomes unstable and changes to an aperiodic behaviour for values lower than $S_v/S_{v_0} = 0.2$ with two unstable real poles. In parallel, as the vertical tail becomes smaller the control effort will be increased to maintain handling quality. Therefore, an optimal trade-off between vertical tail surface area and handling quality at the cost of a reasonable control effort should exist.

2.7 Linear Fractional Representation

Using the previously described modeling, a collection of lateral linear systems $[\mathbf{A}_{D,j}, \mathbf{B}_{D,j}]$ for values of the vertical surface area ranging from $0.1S_{v,0}$ to $1.5S_{v,0}$, with steps of $0.1S_{v,0}$ are computed. The collection of models is then put into a $\mathbf{M} - \boldsymbol{\Delta}$ form (or Linear Fractional Representation LFR). The toolbox APRICOT and the Matlab function `lsapprox` are used to this end. See Clement Roos (2014) for more details about the APRICOT toolbox. The degree of the polynomial chosen is 3 in order to keep the maximum root-mean-square error lower than 1% which
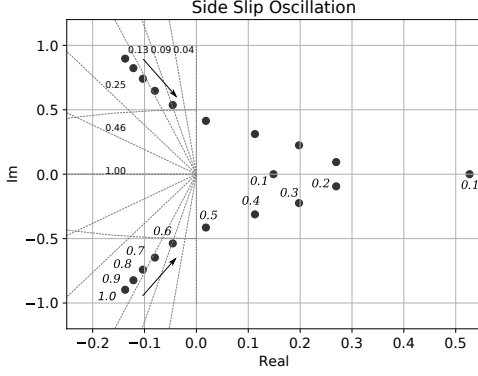
Fig. 2. Evolution of the eigenvalues of the side slip oscillation of the reference aircraft with the reduction of the vertical tail surface area, from $S_\mathrm{v}/S_{\mathrm{v}_0} = 1$ to $S_\mathrm{v}/S_{\mathrm{v}_0} = 0.1$. The number in italic next to an eigenvalue indicates the corresponding quantity $S_\mathrm{v}/S_{\mathrm{v}_0}$. The regular number next to a dashed line corresponds to the damping value.

is quite sufficient at this preliminary design phase. Then $\mathbf{\Delta} = \delta_v\,\mathbf{1}_6$ where $\delta_v = S_\mathrm{v}/S_{\mathrm{v}_0}$ is the tail surface ratio, varying between 0.1 to 1.5 and $\mathbf{1}_n$ is the $n \times n$ identity matrix.

3. CO-DESIGN

3.1 Control architecture

The longitudinal/lateral flight control law is depicted in Figure 3 and involves:

- a static feed-forward gain $\mathbf{H}_L$ $(2{\times}2)$, resp. $\mathbf{H}_D$ $(2{\times}2)$ and a static feedback gain $\mathbf{K}_L$ $(2{\times}2)$, resp. $\mathbf{K}_D$ $(2{\times}4)$, for the longitudinal, resp. lateral, flight control,
- a longitudinal inner loop to control the short period mode through the gains K_α and K_q,
- the symmetrical thrust and differential thrust allocation matrices $\mathbf{L}_L$ (6×1) and $\mathbf{L}_D$ (6×1), respectively.

This set of gains (in green boxes in Figure 3) are the control decision variables $\mathcal{K}$ to be tuned by the optimization process:

$$\mathcal{K} = \{\mathbf{H}_L, \mathbf{H}_D, \mathbf{K}_L, \mathbf{K}_D, K_\alpha, K_q, \mathbf{L}_L, \mathbf{L}_D\}\,.$$

The whole allocation matrix, for the 12 throttle commands, reads:

$$\mathbf{A}_{12\times2} = \begin{bmatrix} \mathbf{1}_6 & \mathbf{1}_6 \\ \mathbf{P}_6 & -\mathbf{P}_6 \end{bmatrix} \begin{bmatrix} \mathbf{L}_L & \mathbf{0}_{6\times1} \\ \mathbf{0}_{6\times1} & \mathbf{L}_D \end{bmatrix},$$

where the permutation matrix $\mathbf{P}_n$ is defined by:

$$\mathbf{P}_n(i,j) = \begin{cases} 1 \text{ if: } i + j = n + 1, \\ 0 \text{ otherwise.} \end{cases}$$

In addition, $\mathbf{S} = \mathrm{diag}([1, \frac{1}{V}, \frac{\pi}{180}, \frac{\pi}{180}])$ is an input shaping gain to take into account the reference input on vertical velocity $V_z \approx V\gamma$ since requirements specify decoupling between V and V_z (see for example Döll et al. (1997)), the side slip and bank angle reference inputs $\widetilde{\beta}_r$ and $\widetilde{\phi}_r$ are expressed in degrees. Thus, a unitary step on each of the 4 components of the reference input $\mathbf{w}$ is expected to create roughly the same thrust magnitude.

The aircraft (A/C) and avionics block of Figure 3 is detailed in Figure 4. It consists of the longitudinal and lateral models presented in the previous section completed by the avionics model between the required control signals $\widetilde{d}_e$, $\widetilde{d}_a$, and $\widetilde{d}_{x,i}$ $(i = 1, \cdots 12)$ computed by the control law and the really applied actuations $\widetilde{\delta}_e$, $\widetilde{\delta}_a$ and $\widetilde{\delta}_{x,i}$. This avionics block considers a second order model on each of the 14 actuators with a damping ratio of 0.7 and a cut-off frequency of ω_e, ω_a and ω_p on the elevator, the ailerons and the 12 propeller engines, respectively. Thus, 2 additional decision variables are added for the optimization process: the vertical tail surface ratio δ_v (6 occurrences) and the propeller engine bandwidth ω_p (24 occurrences).
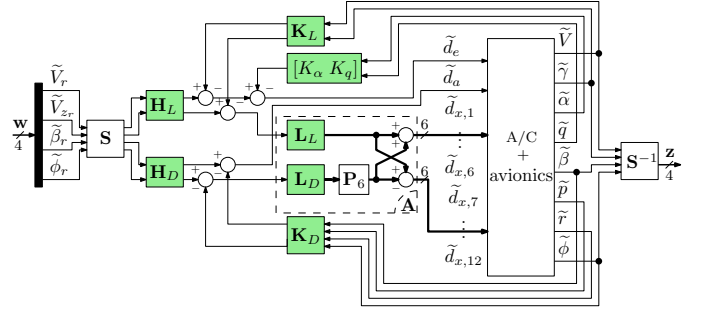

Fig. 3. The longitudinal/lateral closed-loop control block-diagram.
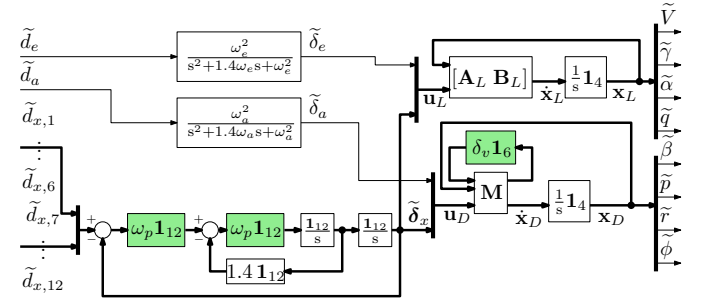

Fig. 4. The A/C + avionics block-diagram.

3.2 Requirements and objectives

The handling qualities are expressed through frequency-domain templates $\mathbf{S}_{o,des}(i,j)$ $(i,j = 1,2,3,4)$ on each element of the 4×4 output sensitivity function $\mathbf{S}_o(\mathrm{s}) = \mathbf{1}_4 - \mathbf{T}_{\mathbf{w}\to\mathbf{z}}(\mathrm{s})$ where $\mathbf{T}_{\mathbf{w}\to\mathbf{z}}(\mathrm{s})$ is the closed-loop transfer between $\mathbf{w}$ and $\mathbf{z}$ as depicted in Figure 3:

$$\gamma_1 = \max_{i,j=1,2,3,4} \left\| \frac{\mathbf{S}_o(i,j)}{\mathbf{S}_{o,des}(i,j)}(\mathrm{s}) \right\|_\infty \leq 1, \qquad (30)$$

with:

$$\mathbf{S}_{o,des}(i,j) = \begin{cases} \dfrac{1.4\,\mathrm{s}}{\mathrm{s} + \omega_i}, \text{ if: } i = j, \\ 0.14, \text{ otherwise.} \end{cases} \text{ and :}$$

$$\omega_1 = 0.2, \ \omega_2 = 0.3, \ \omega_3 = \omega_4 = 1\,(rd/s)\,.$$

Such a multivariate template allows to prescribe low-frequency disturbance rejection and reference input tracking inside the bandwidths $\omega_1,.. \omega_4$ for the servo-loops on V, V_z, β and ϕ, respectively, while ensuring cross couplings to be lower than 14%.

To avoid too high gains in the feed-forward path of the control law and so to reduce as much as possible the thrust magnitude in response to reference inputs, the decision variables must be tuned in order to minimize the maximum of the 12 closed-loop propeller transfers $\mathbf{T}_{\mathbf{w}\to\widetilde{d}_{x,i}}$:

$$J_1 = \max_{i=1,\cdots 12} \left\| \mathbf{T}_{\mathbf{w}\to\widetilde{d}_{x,i}}(\mathrm{s}) \right\|_\infty . \tag{31}$$

Minimizing the objective function J_1 defined in (31) under the constraint defined in (30) is now common in the field of H_∞ structured control design thanks to non-smooth optimization tools (Apkarian (2012)). The challenge here is to minimize also the sizing parameters δ_v and ω_p using 2 additional objective functions:

$$J_2 = \delta_v \quad \text{and} \quad J_3 = \omega_p . \tag{32}$$

3.3 Multi-step optimization process

The multi-step process described below splits the initial multi-objective optimization problem into several consecutive single objective optimization problems where the previous reached objectives are constrained to stay inside a given sub-optimal solution set for the next optimization step. That allows to better understand the optimization process and to manage the trade-off between the various objective functions which is particularly useful during the preliminary design phase. Furthermore, such an approach is also justified since the various objectives J_1, J_2 and J_3 have not normalized units.

Step 0: Initialization. The decision variables are initialized in the following way:

- the initial A/C configuration is defined by $\delta_v = 0.8$ and the avionics are assumed perfect,
- the allocation matrix $\mathbf{A}$ is initialized with: $\mathbf{L}_L = [0,0,0,0,0,1]^T$, $\mathbf{L}_D = [1,0,0,0,0,0]^T$ in such a way that symmetrical thrust uses only inner propellers 6 and 7 and differential thrust uses only outer propellers 1 and 12,
- then, K_α and K_q are designed to assign the short-period mode to the roots of $\left(\frac{\mathrm{s}}{1.2}\right)^2 + 1.4\frac{\mathrm{s}}{1.2} + 1$ on the 2-nd order short-term longitudinal model (also called $(\alpha - q)$ model),
- $\mathbf{K}_L$ is designed to assign the eigenstructure of the longitudinal long-term model (also called $(V - \gamma)$ model), *i.e.* place the 2 corresponding eigenvalues to -0.2 and -0.3 while decoupling the associated eigenvectors from γ or V respectively. See more details in Döll et al. (1997). $\mathbf{H}_L$ is then computed to have an identity DC-gain between $[\widetilde{V}_r, \widetilde{\gamma}_r]^T$ and $[\widetilde{V}, \widetilde{\gamma}]^T$ on this $(V - \gamma)$ model,
- $\mathbf{K}_D$ is designed to assign the 4 eigenvalues of the lateral model to $-1 \pm j$, resp. $-1, -20$, and the associated eigenvectors decoupled from ϕ, resp. β. See more details in Döll et al. (1997). $\mathbf{H}_D$ is then computed to have an identity DC-gain between $[\widetilde{\beta}_r, \widetilde{\phi}_r]^T$ and $[\widetilde{\beta}, \widetilde{\phi}]^T$,
- Finally, the actuators are initialized with $\omega_p = \omega_e = \omega_a = 20\,rd/s$.

Step 1: Optimization on the initial A/C configuration. This optimization aims to meet the constraint (30) while minimizing J_1 using the control decision variables $\mathcal{K}$:

$$\widehat{\mathcal{K}} = \arg \min_{\mathcal{K}} J_1, \text{ s.t. (30) holds.}$$

Let us denote $\widehat{J}_{i,j}$ the optimal value of J_i obtained at step j. Thus $\widehat{J}_{1,1} = \min_{\mathcal{K}} J_1$.

Step 2: Vertical tail minimization. This step aims to minimize the vertical tail surface J_2 while meeting the constraint (30) and keep the objective function J_1 lower than a sub-optimal value $\bar{J}_1 > \widehat{J}_{1,1}$:

$$\{\widehat{\mathcal{K}}, \widehat{\delta}_v\} = \arg \min_{\mathcal{K},\delta_v} J_2, \text{ s.t. (30) holds and } J_1 \le \bar{J}_1.$$

Step 3: Engine bandwidth minimization. This step aims to minimize the engine bandwidth J_3 while meeting the constraints of step 2 and keep the objective function J_2 lower than a sub-optimal value $\bar{J}_2 > \widehat{J}_{2,2}$:

$$\{\widehat{\mathcal{K}}, \widehat{\delta}_v, \widehat{\omega}_p\} = \arg \min_{\mathcal{K},\delta_v,\omega_p} J_3, \text{ s.t. (30) holds and}$$

$$J_1 \le \bar{J}_1, \quad J_2 \le \bar{J}_2 .$$

$\bar{J}_1$ and $\bar{J}_2$, respectively chosen after step 1 and step 2, can be seen as sub-optimality tolerances required to relax the optimality obtained at the previous step in order to add a new objective at the current step.

4. RESULTS

In this section, the results presented are obtained with $\bar{J}_1 = 0.2$ and $\bar{J}_2 = 0.4$. These values are justified by the big gap between $\widehat{J}_{1,0} = 0.713$ and $\widehat{J}_{1,1} = 0.130$ (resp. $\widehat{J}_{2,1} = 0.8$ and $\widehat{J}_{2,2} = 0.1$) presented in Table 2. This Table presents the evolution of the hard constraint γ_1 and the 3 objective functions J_1, J_2 and J_3 after each step of the optimization process. It is worth to mention that the initialization does not meet the hard constraint when the full model and avionics are taken into account. As expected, a trade-off between J_2 and J_3 has to be managed. The obtained solution allows the vertical tail surface to be reduced in a significant way $(\widehat{\delta}_v = 0.4)$ while using a low propeller engine bandwidth $\widehat{\omega}_p = 6.74\,rd/s$.

Table 2. Constraint γ_1 and objective function values during optimization process.

step	γ_1	J_1	$J_2 = \delta_v$	$J_3 = \omega_p\ (rd/s)$
0	1.107	0.713	0.8	20
1	0.999	0.130	0.8	20
2	0.984	0.188	0.1	20
3	0.999	0.199	0.4	6.73

The obtained optimal allocation matrix $\mathbf{A}$ is represented on the bar-diagram of Figure 5. As expected, symmetrical thrust uses mainly inner engines while differential thrust takes benefit of the lever-arm effect and uses mainly outer ones. In addition, Figure 6 displays the bar-diagram of the direct feed-through from the 4 reference inputs (vector $\mathbf{w}$) to the 12 throttle commands $\widetilde{d}_{x,i}$:
$\mathbf{A} \begin{bmatrix} \mathbf{H}_L(2,:) & \mathbf{0}_{1\times 2} \\ \mathbf{0}_{1\times 2} & \mathbf{H}_D(2,:) \end{bmatrix} \mathbf{S}$. Obviously, the most demanding maneuvers from the total thrust magnitude point of view are the forward velocity $\widetilde{V}_r$ and the side-slip angle $\widetilde{\beta}_r$.
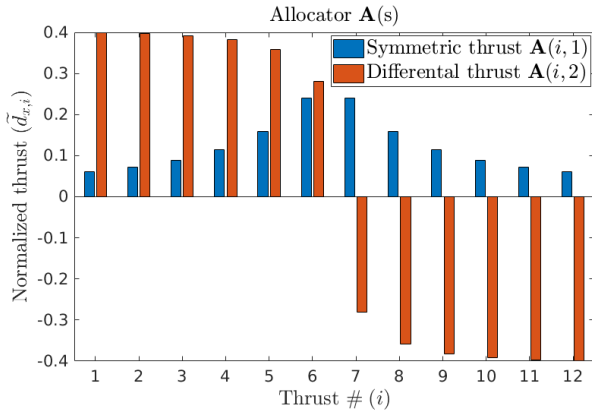
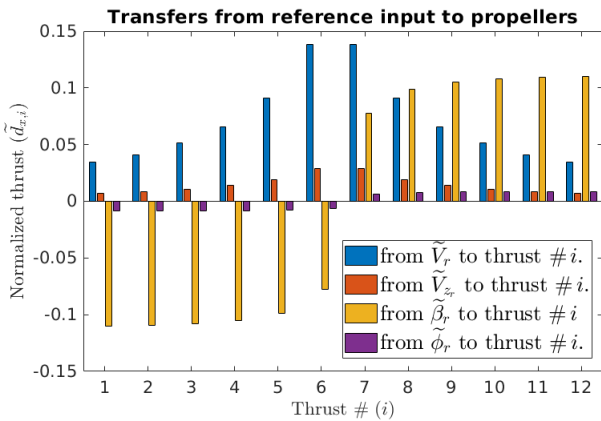Fig. 5. Bar-diagram of the allocation matrix **A**.

Fig. 6. Bar-diagram of the direct feedthrough from reference input to throttle commands.

5. CONCLUSION

An aircraft model using distributed electrical propulsion parameterized according to the vertical tail surface and propeller engine bandwidth was developed and used to co-design the full axes control law of a reduced-tail/without rudder configuration using low actuator bandwidths. The optimization process allows main trade-offs to be managed during the preliminary design phase. Further developments to consolidate such an approach will be focused on:

- its application to the full flight envelope,
- its experimental validation thanks to an aircraft mock-up using distributed and differential propulsion, currently under progress.

REFERENCES

Apkarian, P. (2012). Tuning Controllers Against Multiple Design Requirements. In *System Theory, Control and Computing (ICSTCC), 2012 16th International Conference on*, 1–6. IEEE.

ATR (2015). Type certificate data sheet no. a53eu.

Boiffier, J.L. (1998). *The Dynamics of Flight*.

Ciliberti, D., Nicolosi, F., and Vecchia, P.D. (2013). A new approach in aircraft vertical tailplane design. *XXII Conference AIDAA*.

Clement Roos, George Hardier, J.M.B. (2014). Polynomial and rational approximation with the APRICOT library of the SMAC toolbox. doi:10.1109/CCA.2014.6981532.

Denieul, Y., Bordeneuve-Guib, J., Alazard, D., Toussaint, C., and Taquin, G. (2017). Multi-control Surface Optimization for Blended WingBody Under Handling Quality Constraint. *Journal of Aircraft*, 55, 638–651.

Döll, C., Magni, J., and Le Gorrec, Y. (1997). A modal multi–modal approach. In J. Magni, S. Bennani, and J. Terlouw (eds.), *Robust flight control — A design challenge*, volume 224, chapter 19, 258–277. 1st edition.

Fabrizio Nicolosi, Perluigi Della Vecchia, D.C. (2013). An investigation on vertical tailplane contribution to aircraft sideforce. *Aerospace Science and Technology*, 28(1), 401 – 416. doi: https://doi.org/10.1016/j.ast.2012.12.006.

Felder, J.L., Kim, H.D., and Brown, G.V. (2009). Turboelectric distributed propulsion engine cycle analysis for hybrid wing body aircraft. *47th AIAA Aerospace Sciences Meeting*, (1132). doi:10.2514/6.2009-1132.

Gloudemans, J.R., Davis, J.D., and Gelhausen, P.A. (1996). A rapid geometry modeler for conceptual aircraft. *AIAA, Aerospace Sciences Meeting and Exhibit, 34th, Reno, NV, Jan. 15-18, 1996*.

Goman, M.G., Khramtsovsky, A.V., and Kolesnikov, E.N. (2008). Evaluation of aircraft performance and maneuvrability by computation of attainable equilibrium sets. *JOURNAL OF GUIDANCE, CONTROL, AND DYNAMICS*, 31(2). doi:10.2514/1.29336.

Hermetz, J., Ridel, M., and Döll, C. (2016). Distributed Electric Propulsion for small business aircraft — A concept-plane for key-technologies investigations. In *Proc. 30th ICAS Congress*. Daejeon, South Korea.

Jackson, P. (2015). Jane's all the world aircraft.

Kraft, D. (1988). *A software package for sequential quadratic programming*. Number DFVLR-FB 88-28 in Forschungsbericht / Deutsche Forschungs- und Versuchsanstalt für Luft- und Raumfahrt. Wissenschaftl. Berichtswesen d. DFVLR.

Moore, M.D. and Fredericks, B. (2014). Misconception of electric propulsion aircraft and their emergent aviation market. *52nd AIAA Aerospace Sciences Meeting*, (0535).

Nguyen-Van, E., Alazard, D., Pastor, P., and Döll, C. (2018a). Reduction of vertical tail using differential thrust: Influence on flight control and certification. *AEGATS'18, Toulouse, France*.

Nguyen-Van, E., Alazard, D., Pastor, P., and Döll, C. (2018b). Towards an aircraft with reduced lateral static stability using electric differential thurst. *AIAA Aviation Forum*.

Oppenheimer, M.W. and David B Doman, P. (2006). Control allocation for overactuated systems. *4th Mediterranean Conference on Control Automation proceedings*, (321).

Sachs, G. (2012). Flight performance issues of electric aircraft. *AIAA Atmospheric Flight Mechanics Conference*, (4727).

Schmollgruber, P., Atinault, O., Cafarelli, I., Dll, C., Franois, C., Hermetz, J., Liaboeuf, R., Paluch, B., and Ridel, M. (2019). Multidisciplinary Exploration of DRAGON: an ONERA Hybrid Electric Distributed Propulsion Concept. *AIAA SciTech Forum*, (AIAA2019-1585). doi:10.2514/6.2019-1585.

Stückl, S. (2015). *Methods for the Design and Evaluation of Future Aircraft Concepts Utilizing Electric Propulsion Systems*. Phd thesis, Technische Universität München.